Wavelength standard at 543 nm and the corresponding $^{127}I_2$ hyperfine transitions

Wang-Yau Cheng and Jow-Tsong Shy

Department of Physics, National Tsing Hua University, Hsinchu 300, Taiwan

Received June 16, 2000

We have constructed two compact iodine-stabilized 543-nm He–Ne lasers and studied the corresponding $^{127}I_2$ hyperfine transitions. The frequency stability of our lasers reaches 6.2×10^{-14} during a 30-s sampling time; and the resettability is less than 2 kHz. The frequency intervals of the hyperfine peaks were measured and the corresponding hyperfine constants were determined. The line width of each main line was measured. The properties of the b_{10} line, which is suggested to serve as the wavelength standard at 543 nm, were investigated in detail for what is to our knowledge the first time. © 2001 Optical Society of America [S0740-3224(00)00912-7]

OCIS codes: 020.2930, 120.3940, 120.4800, 300.1030, 300.3700.

1. INTRODUCTION

In 1983 the meter was redefined as the distance that light travels in 1/299,792,458 s in vacuum.[1] Therefore one can measure a meter by using a frequency-stabilized laser locked to a suitable molecular–atomic transition center.[2] At present, most national standards laboratories use the iodine-stabilized 633-nm He–Ne laser as the primary length standard, and many international comparisons have been made.[3–6] Typically, an iodine-stabilized 633-nm laser has frequency stabilies of $\sim 1.8 \times 10^{-11}$ for a 1-s sampling time and of 1.8×10^{-12} for a 100-s sampling time, and reproducibility is ~12 kHz.[6] The laser's performance is limited by the configuration of the intracavity iodine cell.

After the hyperfine transitions of $^{127}I_2$ in an external absorption cell with an internal-mirror 543-nm He–Ne laser was observed in 1986,[7] the iodine-stabilized green He–Ne laser was investigated in several laboratories[8–14]; it has been used as a wavelength standard since 1992.[15] A compact iodine-stabilized 543-nm laser system with a good signal-to-noise ratio was since demonstrated, and the b_{10} line of the $R(106)28\text{-}0$ transition was suggested as the wavelength standard line for a 543-nm He–Ne laser. The b_{10} line is isolated from other main lines, and it does not suffer interference from cross-over resonances.[14]

In this paper we report the results of our studies of compact iodine-stabilized 543-nm green He–Ne lasers in which we used two similar iodine-stabilized lasers. The frequency stabilities were 3×10^{-13} and 6.2×10^{-14} for 1- and 30-s sampling times, respectively. The resettability[16,17] was less than 2 kHz during one week, and the frequency offset was ~7 kHz. Our results show that the iodine-stabilized green He–Ne laser is superior to the conventional iodine-stabilized 633-nm He–Ne laser.

We also report on our investigations of the corresponding $^{127}I_2$ hyperfine transitions. The frequency intervals of the main lines were measured, and the corresponding hyperfine constants were determined. We also measured the linewidth of each main line. The spectroscopic properties of the suggested length standard line (b_{10}), such as pressure shift, pressure broadening, and the absorption coefficient, were investigated.

2. EXPERIMENTAL SETUP

The setup for our beat-frequency measurement system is shown in Fig. 1. We constructed two similar iodine-stabilized 543-nm He–Ne lasers as described in Ref. 14. Both lasers use Melles Griot 05-LGR323 laser tubes, each of which has a piezoelectric transducer glued into it and a heating tape wrapped about it for modulating and locking the laser frequency, respectively. Each laser is enclosed in a thin aluminum box without temperature regulation. Compared with the other Melles Griot laser tubes used in the research described in Ref. 14, this laser tube has an improved structure such that no adjusting screws or wooden box is needed for maintaining the laser power.

For frequency locking, each laser is modulated at ~23 kHz with a modulation depth of 3 MHz. The modulation frequencies of the two lasers differ by ~1 kHz. The conventional third-harmonic locking method is used to lock the laser frequency to the iodine hyperfine peak. The temperature of the cold finger of each iodine cell is regulated by a thermoelectric cooler, and the cell wall is maintained at room temperature. The reader should refer to Ref. 14 for details of the frequency locking.

Because laser 1 has 120-μW single-mode power, whereas laser 2 has 270 μW of power, a double Faraday isolator is employed in laser system 2 to eliminate the unwanted modes. We also use lenses of different focal lengths to obtain the same power intensity (0.6 mW/mm^2) in the iodine cells. In addition, the b_{10} line is located at

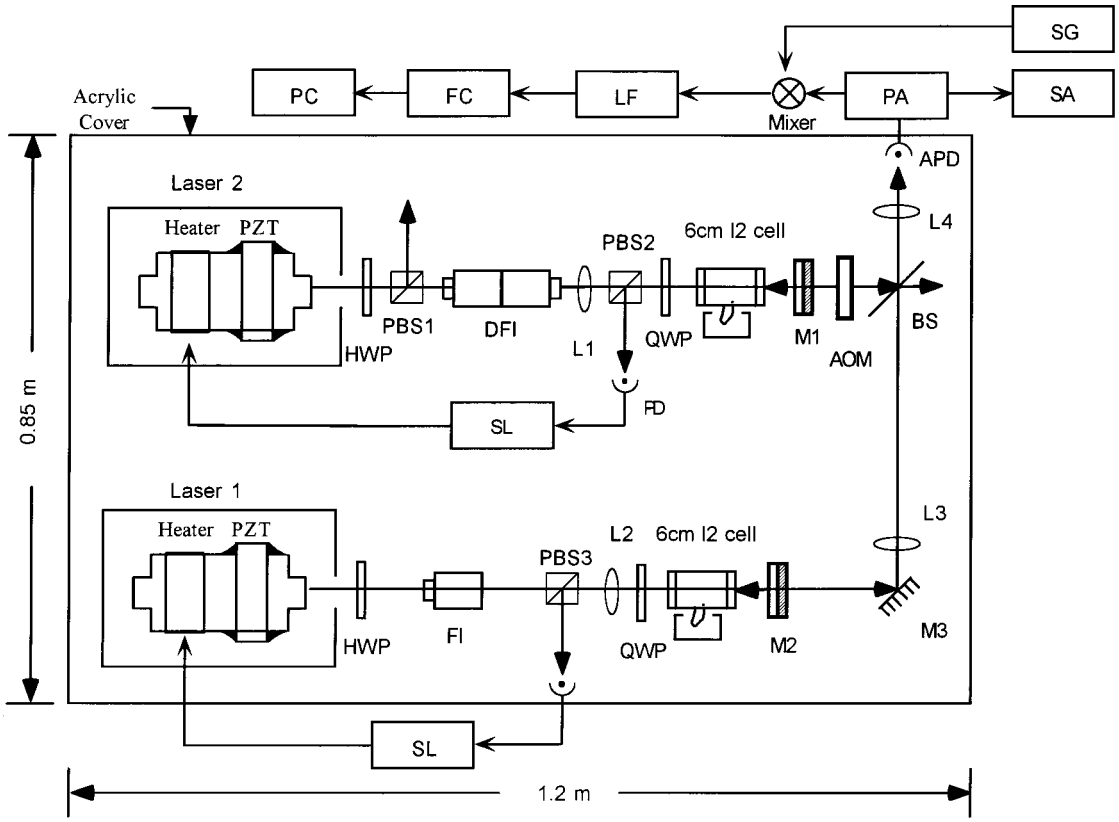

Fig. 1. Schematic diagram of our experimental setup. Each laser is enclosed in a thin aluminum box. PZT's, piezoelectric transducers; HWP's half-wave plates; QWP's, quarter-wave plates; DFI, double Faraday isolator; FI, Faraday isolator; PBS's, polarizing beam splitter's L1, L2, convex lenses of focal lengths 50 and 30 cm, respectively; M1, M2, 90% partial reflection mirrors; M3, total reflection mirror, BS, beam splitter; AOM, 80-MHz acousto-optic modulator; PD, photodiode; APD, avalanche photodiode; PA, preamplifier; SA, spectrum analyzer; SG, signal generator; LF, 10-MHz low-pass filter; FC, frequency counter; SL's servo loops; PC, personal computer.

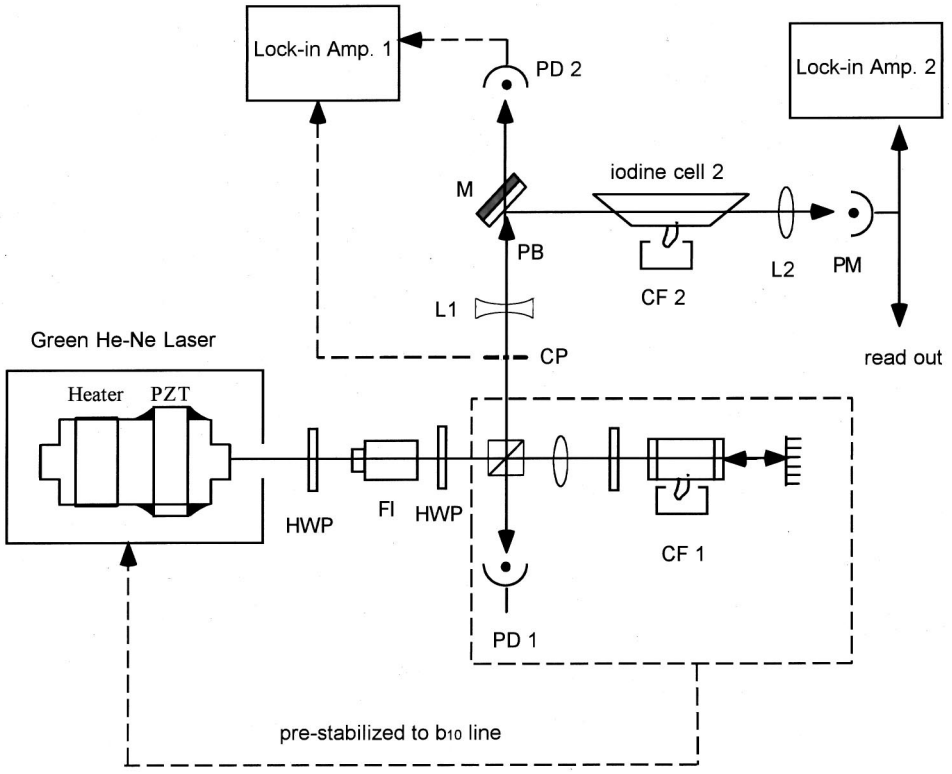

Fig. 2. Experimental arrangement for measuring the absorption coefficient of the b_{10} line. The abbreviations are same as in Fig. 1, except as follows: L1, concave lens ($f = -15$ cm); L2, convex lens ($f = 7$ cm); CF's, cold fingers; CP, chopper; M, partial reflection mirror ($R = 90\%$); PB, probe beam; PM, powermeter.

the wing of the gain profile of laser 1, whereas it is located at the center of the gain profile of laser 2. The third-harmonic demodulated signal for the b_{10} line is approximately two times larger for laser 2. Therefore laser 2 has better stability than laser 1 when both lasers are stabilized to the b_{10} line.

The beat note between lasers 1 and 2 is detected by an avalanche photodiode. First it is amplified by a preamplifier (HP 8447D), and then the beat frequency is down-converted to a frequency of less than 10 MHz by a signal generator (HP 8643A) and a HP 10514A mixer with a 10-MHz low-pass filter (Mini-circuit BLP-10.7) to eliminate the interference from the other longitudinal modes, we measured the beat frequency with a frequency counter (HP 5313A) and recorded it with a personal computer. When both lasers are locked to same hyperfine peaks we use an 80-MHz acousto-optic modulator to shift the frequency of the laser 1 by +80 MHz.

The experimental setup for measuring the absorption coefficient of the b_{10} line is shown in Fig. 2; the laser is locked to the b_{10} line by a third-harmonic locking technique. The probe beam power can be adjusted by use of a half-wave plate, and the laser beam is expanded by a concave lens to ensure a sufficiently weak probe intensity in the iodine cell. The beam radius is 2.75 mm at one Brewster window of the iodine cell and 2.81 mm at the other end. Two lock-in amplifiers are used to measure the probe power, and their readings are calibrated against a Newport Model 815 powermeter. The transmittance of the empty cell is estimated from measurement at a low vapor pressure (~0.4 Pa) by use of relatively high probe power ($100 \sim 170\,\mu$W).

3. EXPERIMENTAL RESULTS

A. Frequency Stability and Resettability

The typical two-sample Allen standard deviation of the beat frequency between our two laser systems is depicted in Fig. 3. Here, laser 1 is locked to b_2 and laser 2 is locked to b_{15}. The cold-finger temperature of both cells is 0 °C. The Allan standard deviation is 3×10^{-13} for a 1-s sampling time and 6.2×10^{-14} for a 30-s sampling time, which verifies the previous estimate[14] based on the signal-to-noise ratio of the saturated absorption signal. Note that we use only the thermal loop to lock the laser. Long-term drift is observed for sampling times longer than 100 s and is probably due to the temperature drift of the cold finger of the iodine cell. The temperature stability of the cold fingers is ±0.05 °C.

There is a 7-kHz frequency offset between the two lasers when they are locked to the b_{10} hyperfine peak. We measured the frequency resettability[16,17] to be less than 2 kHz by measuring the beat frequency between the b_{10} and the b_2 lines for one week.

B. Frequency Intervals and Hyperfine Constants

Table 1 lists the measured frequency differences of the main lines relative to the b_{10} line and also previous results. The average uncertainty of our measurements is ~0.9 kHz. Our measured frequencies are in good agreement with the previous results, especially the results of Brand[11] and Simonsen *et al.*[13]

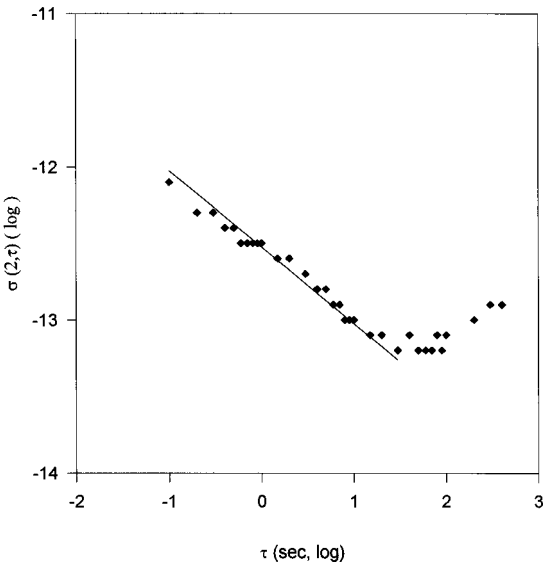

Fig. 3. Two sample Allan standard deviations $\sigma(2, \tau)$ of the beat frequency between the b_{15} and b_2 lines; τ, sampling time. Both horizontal and vertical axes are on a log scale. The solid line is proportional to $1/\tau$.

Precise measurements of the hyperfine splitting of various rovibronic transitions verified that the hyperfine interactions of molecular iodine are caused by nuclear electric quadrupole–surrounding charge distribution interaction (H_{neq}),[18] nuclear magnetic dipole–molecule angular rotation interaction (H_{sr}),[18] "tensor nuclear spin–spin" interaction (H_{tss}),[19] and a scalar nuclear spin–spin interaction (H_{sss}),[18,20–22] and the hyperfine Hamiltonian can be expressed as

$$\begin{aligned} H_{\mathrm{hyperfine}} &= H_{\mathrm{neq}} + H_{\mathrm{sr}} + H_{\mathrm{tss}} + H_{\mathrm{sss}} \\ &= -eqQf(I, J, F) - C\vec{I}\vec{J} - d \\ &\quad \times [(\hat{I}_1\hat{I}_2 - 3(\hat{I}_1\hat{r}_{12})(\hat{I}_2\hat{r}_{12})/r_1^2] + \delta I_1 I_2, \end{aligned}$$

where, $\vec{I}$ denotes the nuclear spin, $\vec{J}$ denotes the orbital angular momentum, $F = I + J$ denotes the coupling angular momentum and I, J, and F are the corresponding quantum numbers, r_{12} denotes the distance between the two nuclei, and eqQ, C, d, and δ are the hyperfine constants. The hyperfine constants can be determined by the measured frequency intervals of the hyperfine structure. The details of the function $f(I, J, F)$ and the interpretation of the hyperfine coupling constants can be found in Ref. 18.

The hyperfine constants determined by the frequency intervals of Table 1 are listed in Table 2, along with the previous results. The program for fitting the hyperfine constants was generously given by S. Fredin-Picard of BIPM.[23] The hyperfine coupling constants of the lower level were taken from a paper by Yokozeki and Muenter.[24] As Table 2 shows, all the results agree very well.

C. Linewidths of Main Lines

By measuring the relationship of the modulation broadening width to the modulation width, one can determine the actual linewidth of each main line by using the result

Table 1. Measured and Fitted Frequency Intervals (in MHz) with Respect to b_{10}[a]

Hyperfine Structure	This Work	Fitted	DFM1[b1]	PTBc[b2]	Lin *et al.*[c]	Brand[d]	Rayman *et al.*[e]	Chartier *et al.*[f]
$R(12)$ 26-0								
a_3			−910.419					
a_4			−853.335					
a_5			−848.131					
a_6			−795.924	−795.913		−795.915	−795.889	
a_7			−752.380	−752.379		−752.379	−752.383	−752.430
a_8			−733.132	−733.131		−733.133	−733.130	−733.160
a_9	−679.4196(7)	−679.4196	−679.417	−679.419		−679.420	−679.404	−679.420
a_{10}	−596.1073(9)	−596.1090	−596.130	−596.133		−596.131	−596.121	−596.170
a_{11}	−485.6164(8)	−485.6158	−485.617	−485.607	−485.545	−485.610	−485.656	−485.663
a_{12}	−746.3475(6)	−476.3495	−476.348	−476.355	−476.402	476.352	−476.358	−476.391
a_{13}	−423.2218(9)	−423.2231	−423.223	−423.227	−423.234	−423.226	−423.231	−423.265
a_{14}	−410.0169(6)	−410.0250	−410.004	−410.014	−410.012	−410.019	−410.019	−410.066
a_{15}	−305.9037(7)	−305.8958	−305.903	−305.907	−305.919	−305.906	−305.917	−305.990
$R(106)$ 28-0								
b_1	−573.7889(18)	−573.7749	−573.767	−573.760		−573.759	−573.774	−573.812
b_2	−320.4573(6)	−320.4601	−320.460	−320.461	−320.465	−320.462	−320.474	−320.515
b_3	−291.5928(6)	−291.6018	−291.593	−291.580	−291.601	−291.585	−291.606	−291.71
b_4	−282.1346(6)	−282.1468	−282.136	−282.149	−282.143	−282.142	−282.148	−282.31
b_5	−253.6716(9)	−253.6715	−253.672	−253.674	−253.677	−253.675	−253.679	−253.53
b_6	−172.6892(7)	−172.6853	−172.690	−172.692	−172.697	−172.692	−172.694	−172.7
b_7	−159.4284(5)	−159.4292	−159.429	−159.425	−159.433	−159.427	−159.429	−159.423
b_8	−127.7527(7)	−127.7559	−127.755	−127.764	−127.761	−127.763	−127.752	−127.759
b_9	−114.5769(8)	−114.5740	−114.577	−114.569	−114.580	−114.573	−114.570	−114.574
b_{10}	0	0	0	0	0	0	0	0
b_{11}	124.8274(9)	124.8291			124.825		124.826	
b_{12}	132.3159(12)	132.3195			132.312		132.318	
b_{13}	154.5148(11)	154.5206			154.511		154.507	
b_{14}	162.6568(10)	162.6571			162.653		162.640	
b_{15}	287.2406(12)	287.2403			287.243		287.226	
Average difference (kHz)		4	4	8	12	8	10	66

[a] The standard uncertainty of to the last digits is given in parentheses. The uncertainties in other studies, which from 1 kHz to a few tens of kilohertz, are not shown. The average difference is the average of the absolute values of the differences with respect to our measured results.
[b1] Ref. 13, Danish Institute of Fundamental Metrology.
[b2] Ref. 13, Physikalisch-Technische Bundesanstalt.
[c] Ref. 12.
[d] Ref. 11.
[e] Ref. 26.
[f] Ref. 9.

of Nakazawa's analysis,[14,25] here the modulation broadening width is defined as the frequency difference between the two side zeros of the third derivative signal. The HWHM of the a_9 component is 0.85 ± 0.05 MHz in this experiment and agrees well with the values given in Refs. 9, 14 and 26. Table 3 lists the linewidths of the main lines that we observed. From Table 3 we conclude that the linewidths for the observed hyperfine components of the $R(12)$ 26-0 transition (a_9 to a_{15}) are approximately the same within our accepted degree of uncertainty, but for the $R(106)$ 28-0 transition (b_1 to b_{15}) the linewidths show some variation. In particular, the b_5 component has the largest linewidth (1.25-MHz HWHM), and its third-harmonic demodulated signal consequently has the worst signal-to-noise ratio. The fifth component of the other transitions has 15 hyperfine components, and the third component of the other transitions has 21 hyperfine components.[27] From Table 3 we find that the linewidth increases when the quantum number of the coupling angular momentum F increases. For example, the b_5 line (largest linewidth) corresponds to $F = 111$ (largest F), whereas the b_5 line (smallest linewidth) corresponds to $F = 103$ (smallest F). Therefore we suspect that the F-dependent spontaneous predissociation broadening[28,29] plays a role in the linewidth-broadening mechanism of the $^{127}I_2$ hyperfine transitions in visible range.

D. Pressure Shift and Linewidth Broadening of the b_{10} Line

One determines the pressure shift by measuring the change in the beat frequency while varying the cold-finger temperature of one iodine cell (Fig. 2) and keeping the other at 0 °C (the corresponding vapor pressure is 4.12 Pa) when both lasers are stabilized to the b_{10} line. Figure 4 shows that the frequency shift is linear with respect to the vapor pressure, with a red shift pressure of -4.3 ± 0.4 kHz/Pa. This implies the existence of an attrac-

Table 2. Fitted Hyperfine Coupling Constants for the $^{127}I_2$ $R(12)$ 26-0 and $R(106)$ 28-0 Transitions[a]

Transition	This Work	Brand[b]	Chartier *et al.*[c]
$R(12)$ 26-0			
ΔeqQ (MHz)	1917.62(7)	1917.76(1)	1917.70(5)
ΔC (kHz)	59.1(2)	59.13(1)	59.21(12)
Δd (kHz)	−35(2)	−28.3(3)	−26.1(1.1)
$\Delta\delta$ (kHz)	−15(3)	−8.7(2)	−11.0(1.6)
Standard deviation (kHz)	8.1	5.6	6

$R(106)$ 28-0		Lin[d]		
ΔeqQ (MHz)	1914.452(14)	1914.4320(86)	1914.422(7)	1912.96(47)
ΔC (kHz)	70.268(8)	70.267(3)	70.30(1)	70.71(17)
Δd (kHz)	−34.6(6)	−33.9(3)	−34.0(14)	1.58(5)
$\Delta\delta$ (kHz)	−6.7(9)	−9.6(4)	−8.6(3)	−3.66(3)
Standard deviation (kHz)	6.8	2.3	5.4	44

[a] The lower-level constants are the following: $eqQ'' = -2452.5837$ MHz, $C'' = 3.162$ kHz, $d'' = 1.58$ kHz, and $\delta'' = 3.66$ kHz. Here, $\Delta eqQ = eqQ' - eqQ''$ = high level–low level, and similarly for Δc, Δd, and $\Delta\delta$.
[b] Ref. 11.
[c] Ref. 22.
[d] Ref. 12.

Table 3. HWHM Linewidth of the Hyperfine Transitions at 4.12-Pa Vapor Pressure[a]

Hyperfine line	a_9	a_{10}	a_{11}	a_{12}	a_{13}	a_{14}	a_{15}	b_1	b_2	b_3	b_4	b_5	b_6	b_7	b_8	b_9	b_{10}	b_{11}	b_{12}	b_{13}	b_{14}	b_{15}
Quantum number F	13	9	14	12	17	10	11	107	103	106	108	111	104	105	109	110	107	105	106	108	109	107
Linewidth (MHz)	0.85	0.8	0.85	0.85	0.9	0.9	0.9	0.9	0.85	0.9	0.95	0.125	0.85	0.9	1.00	1.05	0.85	0.85	0.85	0.95	0.95	0.9

[a] F is the quantum number that corresponds to the coupling angular momentum F (see text). The a lines are $R(12)$ 26-0 hyperfine transitions, and the b lines are $R(106)$ 28-0 hyperfine transitions.

tive force during collisions between iodine molecules.[30] For comparison, Brand obtained a pressure shift of −3 kHz/Pa for the a_9 line.[11]

We also measured the pressure dependence of the linewidth of the b_{10} line, and the result is shown in Fig. 5. The pressure-broadening effect dominates for pressures of 3.1 to 5.8 Pa, and the pressure-broadening coefficient is 111 ± 5 kHz/Pa. Treating the $^{127}I_2$ vapor as an ideal gas at high vapor pressure is not appropriate because the predissociation rate and the van der Waals force, among other effects, will increase when the vapor pressure is increased.[28,29,31] The power-broadening effect will be dominant for low vapor pressure. Therefore the slope mentioned above cannot be attributed to the collision effect only, and the linear fit in Fig. 5 should be considered an approximation.

E. Absorption Coefficient and Saturation Intensity of the b_{10} Line

The absorption coefficient of the b_{10} line is determined by use of the experimental arrangement shown in Fig. 2. In Fig. 2 the frequency of the laser is locked to the b_{10} line. To determine the absorption coefficient of the b_{10} transition we measure the ratio of the laser power after an iodine cell (I_o) to the laser power before the iodine cell (I_i), that is, I_o/I_i, which is related to the absorption coefficient as

$$I_o/I_i = T\exp(-\alpha PL),$$

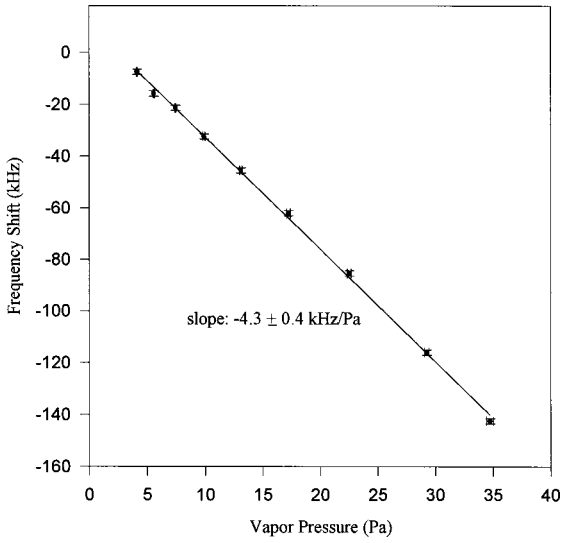

Fig. 4. Pressure shift of the b_{10} line.

where α is the intensity absorption coefficient per unit pressure, T is the transmittance of the empty iodine cell, L is the absorption length (0.095 m), and P is the iodine vapor pressure. We obtain the intensity absorption coefficient $\alpha = 0.33 \pm 0.03\,\mathrm{m^{-1}\,Pa^{-1}}$ by fitting the dependence of I_o/I_i to vapor pressure P under a weak-field interaction. Note that this measured absorption coefficient receives contributions from other hyperfine transitions near b_{10}.

The absorption coefficient of a Doppler-broadened transition can be expressed as[32]

$$\alpha = \alpha_0 \sqrt{\pi}\gamma_2/\gamma_g \exp - (\Delta\omega/\gamma_g)^2,$$

where α_0 is the Doppler-free line-center absorption coefficient, $\Delta\omega$ is the detuning, and γ_2 and γ_g are the Lorentzian and Doppler linewidths, respectively.

Inasmuch as all hyperfine peaks have approximately the same-sized absorption signal, it is reasonable to assume that $\alpha_0\gamma_2$ is the same for all the hyperfine transitions within the Gaussian linewidth of the b_{10} line (including a_{15}, which is on the wing of the linewidth). Then α can be expressed as

$$\alpha = \alpha_0 \sqrt{\pi}\gamma_2/\gamma_g \sum_{i=b2}^{i=b15} \exp-(\Delta\omega_i/\gamma_g)^2$$

$$= \alpha_0 \sqrt{\pi}\gamma_2/\gamma_g \times 8.3173.$$

For the b_{10} line, γ_2 and γ_g have values of 0.85 and 215 MHz, respectively; thus $\alpha_0 = 5.6 \pm 0.6\,\mathrm{m^{-1}\,Pa^{-1}}$.

Because $\alpha_0 = 4\pi^2 Np^2/Ph\varepsilon_0\lambda\gamma_2$, we can estimate the dipole transition moment p of the b_{10} line. Here N is the density of the lower level, p is the dipole transition moment, P is the vapor pressure, h is Planck's constant, ε_0 is the permittivity of vacuum, and λ is the wavelength of the transition. Note that $N = CP/kT$, in which C is the probability of occupation of the lower state. The value of C is estimated to be $\sim 1.8 \times 10^{-4}$ from the formulas of the probabilities of occupation for rotational and vibrational levels given in Refs. 31 and 33, respectively, and assuming that each hyperfine component has a 1/15 population. The estimated dipole transition moment is 9.3×10^{-32} coulomb m.

We obtained saturation intensity I_s, which is 385 $\pm$ 142 μW/mm^2 at 4.12 Pa, by fitting the dependence of the absorption coefficient to the probing power. The ratio of saturation intensity to vapor pressure is shown in Fig. 6. The saturation intensity of the b_{10} line is comparable with the saturation intensities of the $R(56)$ 32-0 hyperfine transitions at 532 nm (314 $\pm$ 3 μW/mm^2; Ref. 34) and the $R(47)$ 9-2 hyperfine transitions at 612 nm [425 $\times$ $(1 + 0.214P)^2$ μW/mm^2, where P is vapor pressure].[35]

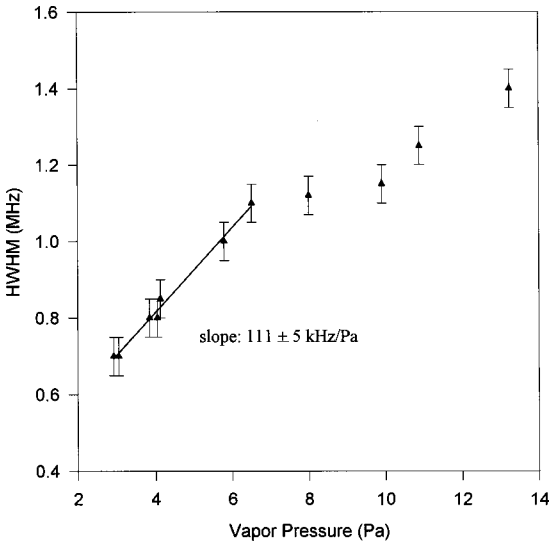

Fig. 5. HWHM linewidth versus vapor pressure for the b_{10} line.

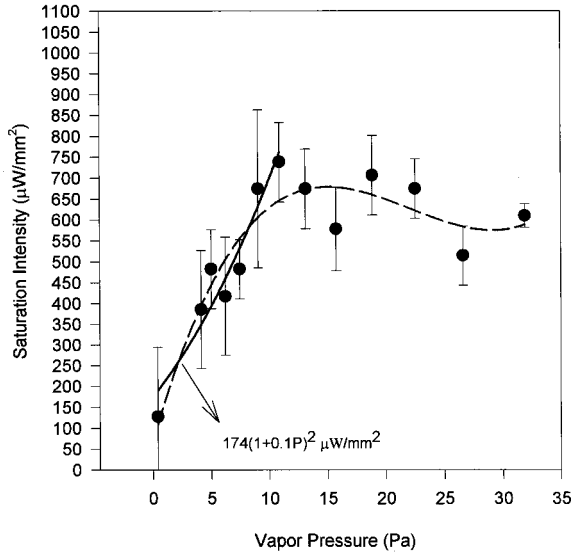

Fig. 6. Saturation intensity versus vapor pressure of $^{127}I_2$. Solid curve, $175(1 + 0.1P)^2\mu$W/mm^2; P, vapor pressure. The dashed curve is a cubic polynomial.

Table 4. Properties of the b_{10} Line[a]

Linewidth (HWHM) at 4.12 Pa	0.85 ± 0.05 MHz
Natural linewidth (HWHM)	0.25 ± 0.1 MHz
Dipole transition moment p	9.3×10^{-32} coulomb m
Pressure shift	−4.3 ± 0.4 kHz/Pa
Pressure broadening ($P < 6$ Pa)	111 ± 5 kHz/Pa
Weak-field absorption coefficient α	0.33 ± 0.03 $\mathrm{m^{-1}\,Pa^{-1}}$
Doppler-free weak-field absorption coefficients α_0	5.6 ± 0.4 $\mathrm{m^{-1}\,Pa^{-1}}$
Saturation intensity (for $P < 11$ Pa)	$174(1 + 0.1P)^2$ W/m^2 (or μW/mm^2)

[a] P is the iodine vapor pressure.

As is shown in Fig. 6, one can easily recognize that, for vapor pressures below 11 Pa, the saturation intensity increases as pressure increases, and it can be fitted by use of the $175 \times (1 + 0.1P)^2$ μW/mm^2 transition (solid curve). However, when the vapor pressure is higher than 11 Pa, the saturation intensity is not an increasing function of vapor pressure, and the data are fitted by use of a cubic polynomial (dashed curve). Furthermore, the linewidth at low vapor pressure can be treated as $\Delta v \sim \Delta v_n \times \sqrt{1 + I/I_s}$, where Δv_n is the natural linewidth. The linewidth of 0.7 MHz at 0.5 Pa (Fig. 5) was obtained for $I \sim 1.1$ mW/mm^2; thus the natural linewidth Δv_n of b_{10} is $\sim$0.25 MHz.

Table 4 summarizes the properties of the b_{10} line obtained in the present study.

4. CONCLUSIONS

We have constructed two compact iodine-stabilized 543-nm He–Ne lasers and studied their frequency stability by measuring the Allan standard deviation of the beat

frequency. The frequency stability is 6.2×10^{-14} for a 30-s sampling time. The frequency resettability is less than 2 kHz. The frequency intervals of the hyperfine structure are measured to an accuracy better than had been achieved previously, and our results are in good agreement with those of earlier studies. The corresponding hyperfine constants are also deduced from the measured intervals.

The properties of the suggested wavelength standard b_{10} line were also investigated. The pressure shift of the b_{10} line was measured to be -4.3 ± 0.4 kHz/Pa (redshift) and the spectroscopic properties of the b_{10} line were determined. The results are summarized in Table 4.

ACKNOWLEDGMENTS

The comments of the referees are gratefully acknowledged. The authors are grateful for support of the National Science Council of the Republic of China under contract NSC 88-2112-M-007-042.

W.-Y. Cheng's e-mail address is chengwy@jilau1.colorado.edu

REFERENCES

1. BIPM, "Documents concerning the new definition of the meter," Metrologia **19**, 163–177 (1984).
2. BIPM, Proc. Verb. Com. Int. Poids et Measures 60, Recommendation 2, CI-1992 (BIPM, Paris, France, 1992).
3. M. Erin, B. Karaboce, I. Malinovsky, A. Titov, H. Ugur, H. Darnedde, and F. Riehle, "Progress in stabilization of the He–Ne/127I2 wavelength standard at 633 nm and results of an international comparison between the PTB and the UME," Metrologia **32**, 301–310 (1995/96).
4. J.-M. Chartier and A. Chartier, "International comparisons of He–Ne lasers stabilized with $^{127}I_2$ at $\lambda \sim 633$ nm (July 1993 to September 1995). I. General," Metrologia **34**, 297–300 (1997).
5. B. Stahlberg, B. Ikonen, J. Haldin, J. Hu, T. Ahola, K. Riski, L. Pendrill, U. Karn, J. Henningsen, H. Simonsen, A. Chartier, and J.-M. Chartier, "International comparisons of He–Ne lasers stabilized with $^{127}I_2$ at $\lambda \sim 633$ nm (July 1993 to September 1995). II. Second comparison of Northern European lasers," Metrologia **34**, 301–307 (1997).
6. V. Navratil, A. Fodrekova, R. Gata, J. Blabla, P. Balling, M. Ziegler, V. Zeleny, F. Petru, J. Lazar, Z. Vesela, J. Gliwa-Gliwinski, J. Walczuk, E. Banrti, K. Tomanyiczka, A. Chartier, and J.-M. Chartier, "International comparison of He–Ne lasers stabilized with $^{127}I_2$ at $\lambda \sim 633$ nm (July 1993 to September 1995). III. Second comparison of Eastern European lasers," Metrologia **35**, 799–806 (1998).
7. J.-M. Chartier, J. L. Hall, and M. Glaser, "Identification of the I_2 saturation absorption lines excited at 543 nm with the external beam of the green He–Ne laser," presented at the Conference on Precision Electromagnetic Measurements, Gaithersburg, Md., June 1986.
8. U. Brand and J. Helmcke, "Frequency stabilization of a 543.5 nm He–Ne laser to an iodine absorption line," in *Proceedings of the Fourth Symposium on Frequency Standard and Metrology*, A. De Marchi, ed. (Springer-Verlag, Berlin, 1989), pp. 467–468.
9. J.-M. Chartier, S. Fredin-Picard, and L. Robertsson, "Frequency-stabilized 543 nm HeNe laser systems: a new candidate for the realization of the meter?" Opt. Commun. **74**, 87–92 (1989).
10. H. Simonsen and O. Poulsen, "Frequency stabilization of an internal mirror HeNe laser at 543.5 nm to I_2-saturated absorptions," Appl. Phys. B **50**, 7–12 (1990).
11. U. Brand, "Frequency stabilization of a HeNe laser at 543.5 nm wavelength using frequency-modulation spectroscopy," Opt. Commun. **100**, 361–373 (1993).
12. T. Lin, Y.-W. Liu, W.-Y. Cheng, J.-T. Shy, B.-R. Jih, and K.-L. Ko, "Iodine-stabilized 543 nm He–Ne lasers," Opt. Commun. **107**, 389–394 (1994).
13. H. R. Simonsen, U. Brand, and F. Riehle, "Intercomparison of two iodine-stabilized He–Ne lasers at $\lambda = 543$ nm," Metrologia **31**, 341–347 (1995).
14. W.-Y. Cheng, J.-T. Shy, and T. Lin, "A compact iodine-stabilized HeNe laser and crossover resonances at 543 nm," Opt. Commun. **156**, 170–177 (1998); W.-Y. Cheng, Y.-S. Chen, C.-Y. Cheng, J.-T. Shy, and T. Lin, "Frequency stabilization and measurements of 543 nm HeNe lasers," Opt. Quantum Electron. **32**, 299–311 (2000).
15. T. J. Quinn, "International reports mise en pratique of definition of the Meter (1992)," Metrologia **30**, 523–541 (1993/1994).
16. J. L. Hall, "The laser absolute wavelength standard problem," IEEE J. Quantum Electron. **QE-4**, 638–641 (1968).
17. H. Sasada and O. Kubota, "Frequency of Lamb-dip-stabilized 1.52 μm He–Ne lasers," Appl. Phys. B **55**, 186–188 (1992).
18. C. H. Townes and A. L. Schawlow, *Microwave Spectroscopy* (Dover, New York, 1975), Chaps. 6–9.
19. N. F. Ramsey, *Molecular Beams* (Oxford U. Press, London, 1956).
20. P. R. Bunker and G. R. Hanes, "Nuclear spin–spin coupling in the spectrum of I_2 at 6328 angstroms," Chem. Phys. Lett. **28**, 377–379 (1974).
21. L. A. Hackel, K. H. Casleton, S. G. Kukolich, and S. Ezekiel, "Observation of magnetic octupole and scalar spin–spin interaction in I_2," Phys. Rev. Lett. **35**, 568–571 (1975).
22. S. Fredin-Picard and A. Razet, "On the hyperfine structure of $^{127}I_2$ lines at the 543 nm wavelength of the HeNe laser," Opt. Commun. **78**, 149–152 (1990).
23. S. Fredin-Picard, "On the hyperfine structure of iodine" report BIPM-90/5 (BIPM, Paris, France, 1990).
24. A. Yokozeki and J. S. Muenter, "Laser fluorescence state selected and detected molecular beam magnetic resonance in I_2," J. Chem. Phys. **72**, 3796–3804 (1980).
25. M. Nakazawa, "Phase-sensitive detection on Lorentian line shape and its application to frequency stabilization of lasers," J. Appl. Phys. **59**, 2297–2305 (1986).
26. M. D. Rayman, M. P. Winters, and J. L. Hall, "Measurement of the hyperfine splittings of the $R(12)26\text{-}0$ and $R(106)28\text{-}0$ transitions in $^{127}I_2$ at 543" (personal communication, JILA, Campus Box 440, University of Colorado, Colo. 80309-0440).
27. J. Ye, L. Robertsson, S. Picard, L. Ma, and J. L. Hall, "Absolute frequency atlas of molecular I_2 lines at 532 nm," IEEE Trans. Instrum. Meas. **48**, 544–549 (1999).
28. A. Brillet, P. Cerez, and C. N. Man-Pichot, *Precision Measurement and Fundamental Constants II*, B. N. Taylor and W. D. Phillips, eds., NBS Spec. Publ. **617**, 73–88 (1984).
29. M. Broyer, J. Vique, and J. C. Lehmann, "Natural hyperfine and magnetic predissociation of the I2 B state. I. Theory," J. Phys. **42**, 937–978 (1981); "Hyperfine predissociation of molecular iodine," J. Chem. Phys. **64**, 4793–4794 (1976).
30. W. Demtroder, *Laser Spectroscopy*, 2nd ed. (Springer-Verlag, Berlin, 1992), Chap. 3.
31. G. Herzberg, Molecular Spectra and Molecular Structure *Spectra of Diatomic Molecules*, 2nd ed., Vol. 1 of (Van Nostrand, Princeton, N.J., 1957), p. 433.
32. P. Meystre and M. Sargent III, *Elements of Quantum Optics*, 2nd ed. (Springer-Verlag, Berlin, 1991), Chap. 5.
33. D. A. McQuarrie, *Statistical Thermodynamics* (University Science, Mill Valley, Calif., 1973), Chap. 6.
34. M. L. Eickhoff and J. L. Hall, "New optical frequency standard at 532 nm," IEEE Trans. Instrum. Meas. **IM-44**, 155–158 (1995).
35. L.-S. Ma and J. L. Hall, "Optical heterodyne spectroscopy enhanced by an external optical cavity: toward improved working standards," IEEE J. Quantum Electron. **26**, 2006–2012 (1990).